1982JApA....3..249S

J. Astrophys. (1982) 3, 249–266

Eclipse Observations of Coronal Emission Lines. I. [Fe x] 6374Å Profiles at the Eclipse of 16 February 1980

Jagdev Singh, M. K. V. Bappu* and A. K. Saxena
Indian Institute of Astrophysics, Bangalore 560034

Received 1982 May 19; accepted 1982 June 28

Abstract. Coronal spectra during the total solar eclipse of 1980 February 16, were obtained in the 6374Å [Fe x] line using a multislit spectrograph. These spectra have a dispersion of 2·5Å mm^{-1}. The observed line profiles from 1·1 to 1·7 $R_{\odot}$ with a spatial resolution of 10×22 $arcsec^2$, give half-widths that vary between 0·6Å and 2·4Å. A large number of locations have half-widths around 1·3Å corresponding to a temperature of $4{\cdot}6 \times 10^6$ K. If temperature of the order of $1{\cdot}3 \times 10^6$ K are typical of the regions that emit [Fe x], then turbulent velocities of $\sim$ 30 km s^{-1} need to be invoked for the enhanced line broadening. The line-of-sight velocities measured range between $+14$ km s^{-1} to -17 km s^{-1}. Most of the locations have velocities less than ± 5 km s^{-1}. From these observations we conclude that corona does not show any localized differential mass motion and that it co-rotates with the photospheric layers deeper down.

Key words: Solar corona — red coronal line — turbulent velocities — rotation of solar corona

1. Introduction

Much information on the physical characteristics of the solar corona can be evaluated from the study of emission-line profiles of the forbidden lines in the coronal spectrum at a total solar eclipse. They permit us to determine the spatial dependence of kinetic temperature or the influence of turbulent velocities that contribute to the enhanced broadening of the line profile. Such studies help us attain an improved understanding of the coronal heating mechanism and the gradients of temperature that contribute to solar wind outflow. The advantage of the total eclipse lies in providing a minimum of scattered-light background and Fraunhofer-line contamination, factors that normally restrict the coronagraph in providing similar information with the aid of an artificial eclipse.

*Deceased on 1982 August 19

© Indian Academy of Sciences • Provided by the NASA Astrophysics Data System

1982JApA....3..249S

Line-profile measures for temperature evaluation have in the recent past been used mostly with coronagraphs. At eclipses, such measures have almost exclusively been carried out with Fabry-Perot interferometers both in the two-dimensional mode by photographic techniques and at a few specific locations by photoelectric scan methods. Such slitless evaluations pioneered by Jarrett and von Klüber (1955, 1961) have been used at subsequent eclipses by Delone and Makarova (1969), Marshall and Henderson (1973), Liebenberg, Bessey and Watson (1975) and Chandrasekhar, Desai and Angreji (1981). The Fabry-Perot instrumentation has the advantage of simultaneous registration of interference fringes over most of the corona, from which a line profile can be evaluated; the disadvantage is the uncertainty of the contribution by Doppler-shifted elements to the line profile and which is inherent in a slitless mode. Such limitations are absent in a slit survey, since the finite width of the slit samples a limited areal extent of the corona. On the other hand, the slit permits the acquisition of information only along the coronal emission regions intercepted by its length, and hence the multiplicity of spatial information collected by the Fabry-Perot technique is missing. Procedures to minimize this handicap, however, do exist and have been used for other purposes at recent solar eclipses (Livingston, Harvey and Doe 1970). The multislit technique has been used by the Kitt Peak investigators only for measures of coronal rotation. It is, however, a technique that can be used to provide a good two-dimensional coverage of the corona by judicious choice of instrumentation and spatial sequencing at the eclipse and has all the advantages to offer which standard slit spectroscopy does over its slitless counterpart.

2. Instruments

An objective of 14 cm aperture and 140 cm focal length formed an image of the sun on the multislit spectrograph. The doublet was corrected for the 6500 Å region and was fed by a single mirror 45-cm coelostat with Zerodur optics, and a well-regulated stepper-motor friction drive. The multislit spectrograph functioned in the Littrow mode with a 600-line grating that gave a dispersion of 2·5 Å mm^{-1} in the fourth order red. Four entrance slits, each separated by 5 mm from its neighbour, together formed the multislit. The slits, therefore, were spaced 12·3 arcmin on the solar image. An interference filter of 9·5 Å pass-band and peaked at 6374 Å was used in front of the multislit. In the Littrow focal plane, four spectra originating from the multislit each about 10 Å in width—were stacked side by side on the photocathode of a single-stage Varo image intensifier. The image intensifier has a gain of 20 and an effective aperture of 30 mm. A plate-holder magazine enabled rapid change-over of the emulsion that had to be in contact with the fibre-optic faceplate. Each spectrum has a neon comparison. Since these spectral lines were not filtered by the interference filter, there were many lines from overlapping orders available that permitted velocity measurements by comparison.

3. Observations

Two of the three plates exposed during the total phase of the eclipse have been used in this study. The third had to be discarded because of excessive tube back-

© Indian Academy of Sciences • Provided by the NASA Astrophysics Data System

1982JApA....3..249S

ground that had accumulated by virtue of the hot afternoon and the fact that the image tube had been turned on in readiness for the event several minutes before totality. The exposures used were both of 45 s duration and enabled emission lines to be detected to distances as far as 1·7 $R_{\odot}$. Between the first and second exposures, the solar image was shifted through 4·5 arcmin along the axis of rotation in order to sample a new set of coronal regions with the multislit. The orientation of the multislit was along position angle 89·5°. The spectra were exposed on Eastman 103a-D emulsion and developed in D-19 at 20°C for five minutes together with the step-wedge calibration obtained immediately after the eclipse with the same spectrograph. Neon spectra obtained along the entire length of the four slits permitted the evaluation of the instrumental line profiles at several points of each slit. We show in Fig. 1 the values of full width at half maximum (FWHM) of these instrumental line profiles at several points on each slit and the final mean value assigned to each for determination of coronal line widths.

Microphotometer scans of these spectra have been obtained with a projected slit size of 4·5 × 22 arcsec^2 on the plate. Successive scans have been made that were separated by 30 arcsec along the slit. This spacing had to be increased to 45 or 50 arcsec at locations where the ratio of maximum line intensity to continuum intensity was low. The transmission curve of the narrow interference filter was evaluated with the aid of the solar spectrum and the Kodaikanal 18-m spectrograph. Working at a

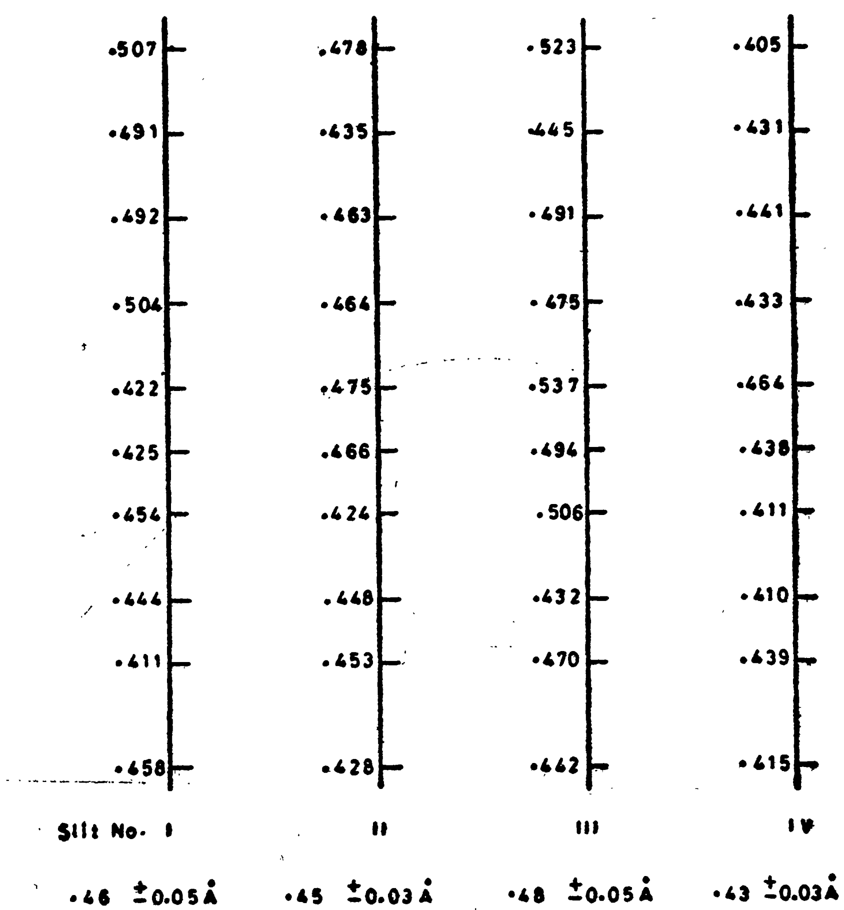

Figure 1. Full width at half maximum of instrumental line profile at various locations on the slits. Mean value is indicated below each slit.

© Indian Academy of Sciences • Provided by the NASA Astrophysics Data System

1982JApA....3..249S

dispersion of 9 mm Å^{-1}, transmission spectra through several different regions of the interference filter—each spaced 5 mm from its neighbour, have been used in the evaluation of the average filter characteristic. The normalized mean transmission curve of the filter thus obtained is used to operate on the intensity curve of the red coronal line, as evaluated at each point along the slit (Fig. 2). The procedure gives the observed profile of the coronal line. The FWHM is corrected for instrumental line-width using the data of Fig. 1 and the assumption that both profiles are gaussian.

Image-tube spectra usually call for extra precautions in radial-velocity measurements over those photographed directly, due to the pin-cushion effect of the image intensifier. We have used the full-length neon spectra and made dispersion measures at several points along the length in terms of a fiducial reference of a cross hair placed against the slits during the eclipse and the measures that followed immediately after. The 6374 Å line was flanked on either side by the neon lines 8495·36 Å (third order spectrum) and 6382·99 Å of the normal fourth order. The Doppler displacements of the line as a whole were evaluated from microphotometer scans that included the neon comparison lines as well. The velocity measures were spaced 30 arcsec along each slit.

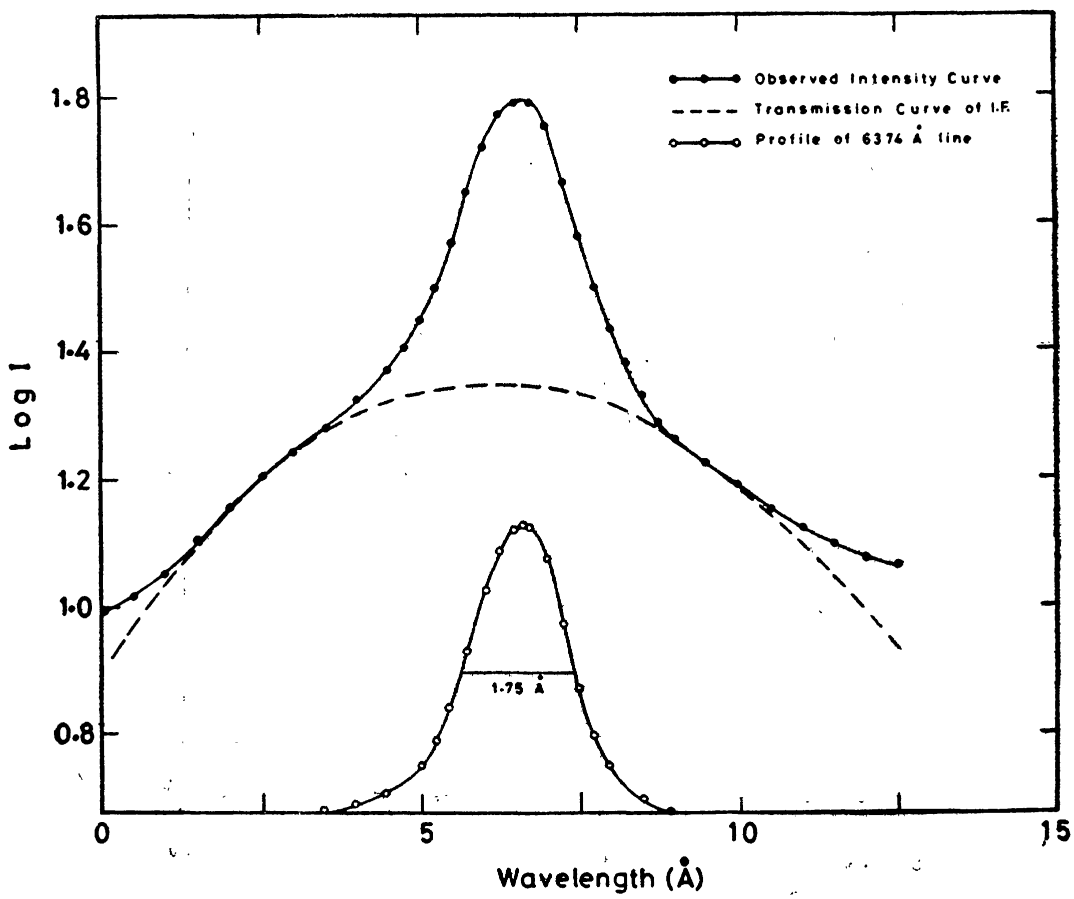

Figure 2. A typical line profile of [Fe x] 6374 Å at one of the locations of corona is shown. Full line is a plot between log I and wavelength whereas the dotted one is the transmission curve of the interference filter on the same scale. Shown below is the line profile plotted as intensity versus wavelength, after correction for the transmission of the interference filter.

© Indian Academy of Sciences • Provided by the NASA Astrophysics Data System

1982JApA....3..249S

4. Results

We have measured the widths of the red coronal line at 236 locations in the solar corona. These locations range from 1·1 $R_\odot$ to 1·7 $R_\odot$ and aim to give a satisfactory coverage all around the solar limb. The data are presented in Table 1. The position angle measured from the north point of the projected axis of solar rotation and the radial distance from the centre of the disc are given in Columns (2) and (3). The values of FWHM are in Column (4) while those in Column (5) express turbulent velocities derived by assuming the temperature of corona to be 1·3 × 10^6 K. In Columns (6) and (7) we give the peak brightness of the continuum at the line centre as well as the peak brightness of the line. This is expressed as a ratio in Column (8) and serves to portray the localized enhancements of the line emission to that of the background K corona.

Table 1. Line widths, intensities and turbulent velocities derived from the red coronal line.

No. (1)	Position angle θ (2)	$R/R_\odot$ (3)	FWHM Å (4)	V_t km s^{-1} (5)	I_c (6)	I_{max} (7)	$\frac{I_{max}}{I_c}$ (8)
			Slit IV (1)				
1	322·9	1·437	1·34	29	19	34	1·79
2	323·4	1·428	1·40	32	18	32	1·78
3	323·9	1·418	1·11	19	22	42	1·91
4	324·4	1·409	1·12	20	19	41	2·16
5	324·9	1·400	1·23	25	25	47	1·88
6	325·4	1·391	1·29	28	23	46	2·00
7	325·9	1·382	1·30	28	29	53	1·83
8	327·0	1·365	1·33	29	31	47	1·52
9	328·1	1·349	1·23	25	47	66	1·40
10	329·2	1·332	1·41	32	54	74	1·37
11	330·3	1·317	1·37	30	59	80	1.36
12	331·5	1·301	1·44	33	67	90	1·34
13	332·7	1·287	1·44	33	68	93	1·37
14	333·9	1·273	1·18	23	77	102	1·32
15	335·2	1·259	1·33	29	81	105	1·30
16	335·5	1·246	1·39	31	83	107	1·29
17	337·8	1·234	1·29	27	91	111	1·22
18	339·1	1·222	0·92	9	98	119	1·21
19	340·5	1·212	1·10	19	101	118	1·17
20	341·8	1·202	1·21	24	105	125	1·19
21	40·0	1·475	1·27	26	22	36	1·64
22	39·1	1·456	1·04	17	22	37	1·68
23	38·1	1·437	1·02	15	25	40	1·60
24	37·1	1·418	1·07	18	28	42	1·50
25	36·1	1·400	1·33	29	31	42	1·35
26	35·1	1·383	1·40	31	34	43	1·26
27	34·0	1·365	1·44	33	39	48	1·23
28	32·9	1·349	1·21	24	43	52	1·21
29	31·8	1·332	1·22	25	48	62	1·29
30	30·7	1·317	1·20	24	53	67	1·26
31	29·5	1·302	1·65	40	57	72	1·26
32	28·3	1·287	1·55	36	62	77	1·24
33	27·1	1·273	1·23	25	74	85	1·15
34	25·8	1·259	1·09	19	79	91	1·15
35	24·5	1·247	1·16	22	85	100	1·18

© Indian Academy of Sciences • Provided by the NASA Astrophysics Data System

1982JApA....3..249S

Table 1. Continued.

No. (1)	Position angle θ (2)	$R/R_\odot$ (3)	FWHM Å (4)	V_t kms^{-1} (5)	I_c (6)	I_{max} (7)	$\frac{I_{max}}{I_c}$ (8)
36	23·2	1·234	1·46	33	89	102	1·15
37	21·9	1·223	1·18	23	94	113	1·20
38	20·5	1·212	1·36	30	96	111	1·16
39	19·2	1·202	1·35	29	106	132	1·25
40	17·8	1·192	1·04	17	108	140	1·30
41	15·6	1·179	1·47	34	107	168	1·57
			Slit IV (2)				
42	308·4	1·403	0·98	13	21	26	1·24
43	310·0	1·355	0·76	1	30	38	1·27
44	312·6	1·285	0·96	12	43	52	1·21
45	313·5	1·263	1·28	27	32	48	1·50
46	314·5	1·240	1·39	31	35	58	1·66
47	315·5	1·218	1·34	29	41	68	1·66
48	316·5	1·197	1·45	33	47	78	1·66
49	318·2	1·165	1·23	25	65	99	1·52
50	319·9	1·134	0·67	0	90	207	2·30
51	322·4	1·096	1·10	19	116	299	2·58
52	324·3	1·068	1·67	40	148	407	2·75
53	56·8	1·553	1·33	29	10	13	1·30
54	56·2	1·528	1·43	32	12	16	1·33
55	55·5	1·502	1·27	26	12	17	1·42
56	54·8	1·477	1·31	28	16	23	1·44
57	54·1	1·452	1·26	26	19	27	1·42
58	53·4	1·428	1·17	22	22	33	1·50
59	52·6	1·403	1·29	27	20	44	2·20
60	51·8	1·379	1·59	38	26	48	1·85
61	51·0	1·355	1·33	29	28	53	1·89
62	50·2	1·332	1·31	28	35	57	1·63
63	49·3	1·308	1·18	23	41	67	1·63
64	48·4	1·285	1·26	26	50	73	1·46
65	47·5	1·263	1·35	29	57	77	1·35
66	46·5	1·240	1·34	29	71	89	1·25
67	45·5	1·218	1·27	26	77	87	1·13
68	44·5	1·197	1·25	26	86	98	1·14
69	43·4	1·176	1·23	25	96	112	1·17
70	42·3	1·155	0·72	0	108	146	1·35
71	41·1	1·135	1·02	15	125	327	2·62
72	39·9	1·115	1·42	32	137	426	3·11
			Slit III (1)				
73	283·9	1·660	2·37	62	8	11	1·38
74	284·2	1·623	1·41	32	10	13	1·30
75	284·5	1·586	1·47	34	10	13	1·30
76	285·0	1·541	1·71	42	14	20	1·43
77	285·3	1·511	1·80	45	14	21	1·50
78	285·6	1·481	1·83	46	17	24	1·41
79	285·9	1·452	1·75	43	21	31	1·48
80	286·2	1·422	1·52	35	28	43	1·54
81	286·5	1·393	1·58	37	35	51	1·46
82	286·9	1·363	1·54	36	41	65	1·59
83	287·4	1·326	1·72	42	53	81	1·53
84	287·9	1·289	1·55	36	71	104	1·46
85	288·3	1·260	1·34	29	85	140	1·65

© Indian Academy of Sciences • Provided by the NASA Astrophysics Data System

1982JApA....3..249S

Table 1. Continued.

No. (1)	position angle θ (2)	$R/R_\odot$ (3)	FWHM Å (4)	V_t km s^{-1} (5)	I_c (6)	I_{max} (7)	$\frac{I_{max}}{I_c}$ (8)
86	76·3	1·571	1·73	42	8	12	1·50
87	76·0	1·541	1·42	32	8	13	1·63
88	75·8	1·511	1·64	40	9	16	1·78
89	75·3	1·467	1·65	40	11	24	2·18
90	75·0	1·437	1·64	40	13	34	2·62
91	74·6	1·407	1·72	42	17	45	2·65
92	74·1	1·363	1·75	43	22	62	2·82
93	73·7	1·334	1·93	49	28	78	2·79
94	73·3	1·304	2·18	57	34	89	2·62
95	72·9	1·275	2·32	61	45	106	2·36
96	72·5	1·245	2·15	56	57	127	2·23
97	72·1	1·216	2·12	55	68	151	2·22
			Slit III (2)				
98	274·4	1·573	1·10	19	6	9	1·50
99	274·5	1·542	1·65	40	6	10	1·67
100	274·6	1·511	1·47	34	7	11	1·57
101	274·7	1·481	1·02	15	9	13	1·44
102	274·8	1·450	1·45	33	10	17	1·70
103	274·9	1·419	1·28	27	12	22	1·83
104	275·0	1·389	1·31	28	16	28	1·75
105	275·1	1·358	1·30	28	22	36	1·64
106	275·2	1·327	1·52	35	28	44	1·57
107	275·3	1·297	1·47	34	35	55	1·57
108	275·4	1·266	1·25	26	50	74	1·48
109	275·5	1·235	1·40	31	71	90	1·27
110	275·6	1·205	1·38	30	86	113	1·31
111	275·8	1·174	0·96	12	106	202	1·91
112	275·9	1·143	1·57	37	132	424	3·21
113	87·0	1·788	1·31	28	5	8	1·60
114	86·9	1·711	0·74	1	6	9	1·50
115	86·7	1·634	1·39	31	7	10	1·43
116	86·6	1·604	0·96	12	7	14	2·00
117	86·6	1·573	1·03	16	9	16	1·78
118	86·5	1·542	1·39	31	8	18	2·25
119	86·4	1·512	1·30	28	10	25	2·50
120	86·3	1·481	1·24	25	10	31	3·10
121	86·2	1·450	1·47	34	12	38	3·17
122	86·1	1·419	1·45	33	14	48	3·43
123	86·0	1·389	1·54	36	19	65	3·42
124	85·9	1·358	1·68	41	25	79	3·16
125	85·8	1·327	1·89	48	36	92	2·56
126	85·7	1·297	1·94	49	37	113	3·05
127	85·6	1·266	1·10	19	56	200	3·57
128	85·5	1·235	1·01	15	70	248	3·54
129	85·4	1·205	1·24	25	93	492	5·29
130	85·2	1·174	1·27	26	104	441	4·24
131	85·1	1·144	1·71	42	124	452	3·65
			Slit II (1)				
132	257·6	1·657	1·92	48	9	11	1·22
133	257·3	1·620	1·28	27	9	10	1·11
134	257·0	1·582	1·79	44	11	13	1·18
135	256·6	1·537	1·19	23	13	17	1·31
136	256·3	1·507	1·56	37	14	19	1·36

© Indian Academy of Sciences • Provided by the NASA Astrophysics Data System

1982JApA....3..249S

Table 1. Continued.

No.	Position angle θ	$R/R_{\odot}$	FWHM Å	V_t km s^{-1}	I_c	I_{max}	$\frac{I_{max}}{I_c}$
(1)	(2)	(3)	(4)	(5)	(6)	(7)	(8)
137	256·0	1·478	1·62	39	18	22	1·22
138	255·7	1·448	2·00	51	21	26	1·24
139	255·4	1·418	1·81	45	31	38	1·23
140	255·1	1·388	1·88	47	39	46	1·18
141	254·7	1·359	1·81	45	52	60	1·15
142	254·3	1·322	1·65	40	72	79	1·10
143	253·8	1·285	1·51	35	93	100	1·08
144	253·4	1·255	1·24	25	110	125	1·14
145	104·1	1·567	1·94	49	12	15	1·25
146	104·4	1·537	20·6	53	12	14	1·17
147	104·7	1·507	1·88	47	13	16	1·23
148	105·1	1·463	2·17	56	14	19	13·6
149	105·4	1·433	2·09	54	18	22	1·22
150	105·8	1·403	2·23	58	21	25	1·19
151	106·3	1·359	2·33	61	25	29	1·16
152	106·6	1·329	2·40	63	29	24	1·17
153	107·0	1·300	1·76	43	34	40	1·17
154	107·4	1·270	1·48	34	43	50	1·16
155	107·8	1·241	1·65	40	49	55	1·12
156	108·2	1·211	1·67	41	57	62	1·19
157	108·7	1·182	1·73	42	72	78	1·08
158	109·2	1·153	1·75	43	76	82	1·08
159	109·9	1·109	1·21	24	91	108	1·19
			Slit II (2)				
160	248·1	1·697	1·94	49	5	8	1·60
161	247·7	1·669	1·32	28	6	9	1·50
162	247·3	1·640	2·09	54	6	9	1·50
163	246·9	1·612	1·72	42	6	10	1·67
164	246·4	1·584	1·35	29	8	12	1·50
165	246·0	1·556	1·17	22	9	15	1·67
166	245·5	1·528	1·32	28	10	19	1·90
167	245·0	1·500	1·65	40	11	24	2·18
168	244·5	1·472	1·90	48	13	31	2·38
169	242·8	1·363	1·91	48	28	77	2·75
170	241·6	1·336	1·44	33	46	92	2·00
171	240·9	1·309	1·50	35	58	103	1·78
172	240·3	1·282	1·34	29	75	126	1·68
173	238·8	1·230	1·13	21	104	333	3·20
174	115·5	1·528	0·68	0	9	15	1·67
175	116·0	1·500	1·20	24	11	19	1·73
176	116·5	1·472	1·55	36	11	18	1·64
177	117·0	1·445	1·52	35	12	21	1·75
178	117·6	1·417	1·68	41	14	28	2·00
179	118·2	1·390	1·88	47	16	33	2·06
180	118·8	1·363	1·70	41	23	43	1·87
181	119·4	1·336	1·57	37	27	47	1·74
182	120·1	1·309	1·71	42	31	54	1·74
183	120·8	1·282	1·51	35	42	63	1·50
184	121·5	1·256	1·52	35	51	71	1·39
185	122·2	1·230	1·17	22	64	79	1·23
186	123·0	1·203	1·27	26	77	84	1·09
187	123·8	1·178	1·43	32	85	96	1·13
188	124·6	1·152	0·69	0	99	114	1·15
189	125·5	1·127	1·10	19	104	127	1·22
190	126·4	1·102	1·38	31	132	256	1·94

© Indian Academy of Sciences • Provided by the NASA Astrophysics Data System

1982JApA....3..249S

Table 1. Concluded.

No.	Position angle θ	$R/R_\odot$	FWHM Å	V_t km s^{-1}	I_c	I_{max}	$\frac{I_{max}}{I_c}$
(1)	(2)	(3)	(4)	(5)	(6)	(7)	(8)
			Slit I (1)				
191	218·5	1·425	2·05	53	40	46	1·15
192	217·5	1·406	2·03	52	42	48	1·14
193	216·5	1·388	1·91	48	48	55	1·15
194	215·4	1·370	2·06	53	49	55	1·12
195	214·4	1·353	1·21	24	53	58	1·09
196	213·3	1·336	1·64	40	53	58	1·09
197	212·2	1·319	2·04	52	57	61	1·07
198	209·2	1·281	1·18	23	66	68	1·03
199	146·1	1·361	1·54	36	17	21	1·24
200	148·8	1·319	2·21	58	20	25	1·25
201	151·8	1·280	2·14	55	26	30	1·15
202	154·9	1·245	2·10	54	32	41	1·28
203	158·2	1·214	2·32	61	47	54	1·15
204	161·6	1·187	1·71	42	62	68	1·10
205	168·9	1·147	1·52	35	93	100	1·08
			Slit I (2)				
206	213·9	1·677	1·35	29	12	17	1·42
207	213·0	1·660	0·72	0	12	18	1·50
208	212·1	1·644	1·23	25	12	17	1·42
209	211·2	1·628	1·61	39	12	16	1·33
210	209·8	1·605	1·44	33	13	19	1·46
211	208·3	1·583	1·42	32	15	22	1·47
212	206·3	1·555	1·45	33	16	25	1·56
213	204·8	1·535	1·28	27	19	26	1·37
214	203·2	1·517	1·56	37	21	28	1·33
215	201·0	1·495	1·31	28	24	28	1·17
216	199·3	1.479	1.10	19	26	32	1·23
217	197·6	1.465	1·32	28	29	36	1·24
218	195·3	1·448	1·74	43	30	38	1·27
219	193·5	1·437	1·25	26	34	38	1·12
220	191·7	1·427	1·54	36	34	40	1·18
221	189·3	1·416	1·72	42	35	41	1·17
222	187·4	1·410	1·20	24	38	41	1·08
223	185·5	1·405	1·03	16	42	45	1·07
224	183·0	1·401	1·10	19	43	54	1·26
225	181·1	1·400	1·28	27	42	50	1·19
226	156·3	1·536	1·13	21	9	10	1·11
227	158·9	1·506	1·33	29	10	13	1·30
228	161·1	1·484	1·72	42	12	16	1·33
229	162·8	1·469	1·23	25	15	20	1·33
230	164·6	1·456	1·68	41	18	23	1·28
231	166·9	1·440	1·36	30	24	32	1·33
232	168·7	1·430	1·45	33	28	36	1·29
233	170·5	1·421	1·93	49	31	38	1·23
234	172·4	1·414	1·23	25	31	40	1·29
235	174·2	1·408	1·52	35	31	39	1·26
236	179·2	1·400	0·96	12	38	42	1·11

© Indian Academy of Sciences • Provided by the NASA Astrophysics Data System

1982JApA....3..249S

4.1 *Line Widths*

The derived values of FWHM of the red coronal line varies between 0·6 Å and 2·4 Å. The values at the different locations are depicted in Fig. 3. One can thus evaluate the association of any line widening with coronal form. When we plot a histogram of line-width dependence, as in Fig. 4, we find a predominance of values of FWHM

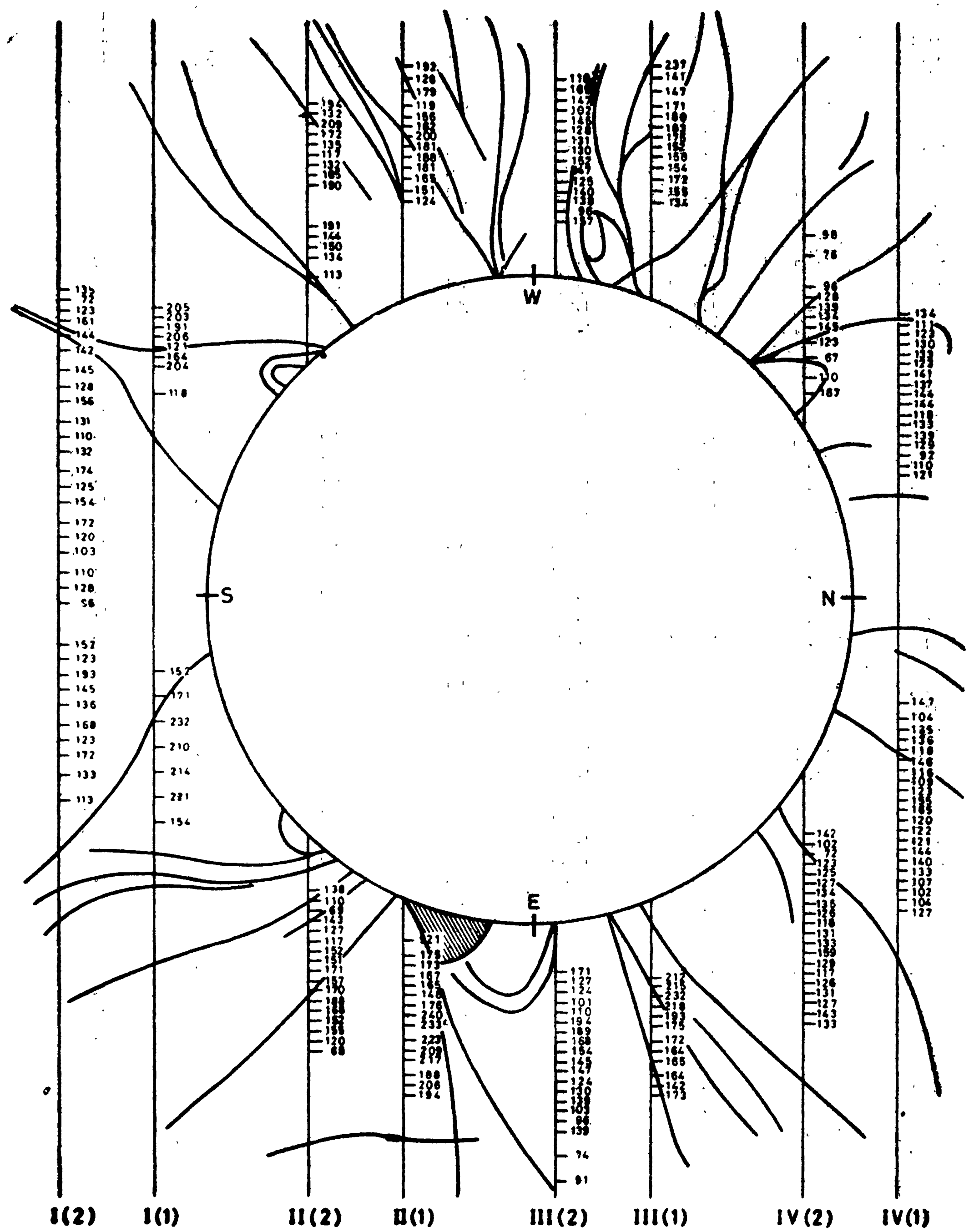

Figure 3. True line widths of [Fe x] 6374 Å line are written at various locations in Å × 10^{-2}. I(1), II(1), III(1) and IV(1) are the slit positions on solar disc with plate 1 and correspondingly with suffix 2 in bracket are due to plate 2. A sketch of white-light corona is super-imposed to compare the two. Shaded area on E-limb is an enhancement observed in white light corona and the horizontal line crossing slit positions II(2) and II(1) is the filament.

© Indian Academy of Sciences • Provided by the NASA Astrophysics Data System

1982JApA....3..249S

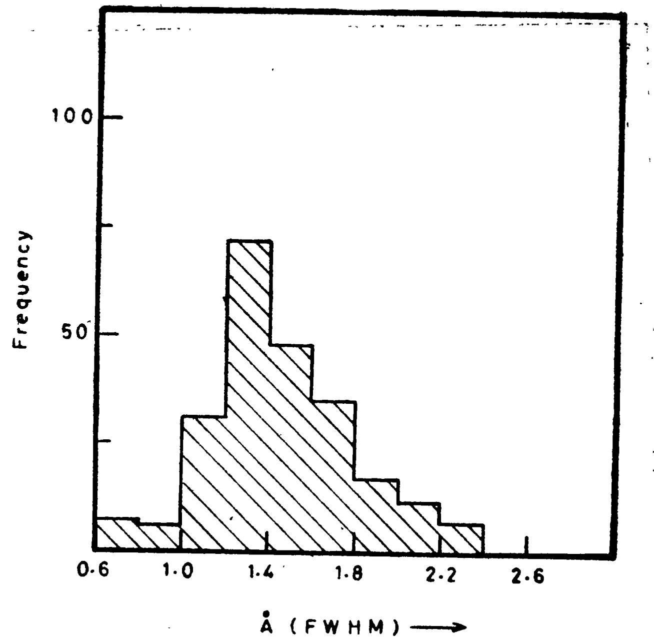

Figure 4. Frequency distribution of true line widths of [Fe x] 6374Å.

around 1·3Å and an extended tail towards larger values. The lowest value of line width is 0·6Å. If thermal broadening is the only contributor to line widths then with the aid of the standard kinetic-temperature formula one derives a temperature of $1{\cdot}2\times10^6$ K for a line width of 0·67Å. The temperature assumes higher values, if one converts the peak of the FWHM of 1·3Å. The value is then $4{\cdot}6\times10^6$ K while the largest value of line width of 2·4Å represents even a higher value of temperature, if one interprets it to be so. Jordan (1969) had calculated the ionization equilibrium as a function of temperature for several of the ions commonly seen in eclipse spectra. Fe x is mostly available in the temperature zone 5×10^5–2×10^6, with a peak at $1{\cdot}3\times10^6$K. It therefore becomes inadmissible to accept the high values of temperature inferred from line widths, especially for a relatively low temperature ion like Fe x. Therefore the need to assume an additional line-broadening agency seems necessary. Introducing a turbulence parameter in the equation, and assuming the ions of iron to be controlled by the peak value of $1{\cdot}3\times10^6$ K (Jordan 1969), one finds turbulent velocities of 30 km s^{-1} from line broadening. The smallest values in the histogram of line widths seems to be representative of the state of ionization. The larger FWHM must necessarily signify the appreciable contribution to it by Doppler motion. An evaluation of this characteristic is extremely difficult. For, in the line of sight of an optically thin gas, we witness—besides the effects of thermal broadening—several other factors. The presence of broadening by random motions is clear. The value of 30 km s^{-1} is in good accord with that derived by Delone and Makarova (1969). The advantages of similar studies at future eclipses, based on simultaneous exposures of lines of at least two different atomic weights, are obvious.

4.2 *Line and Continuum Intensities*

Our measures of intensity, both at the peak of the line and at the underlying continuum, can be used for the study of gradients of both the emission corona and the K corona.

© Indian Academy of Sciences • Provided by the NASA Astrophysics Data System

1982JApA....3..249S

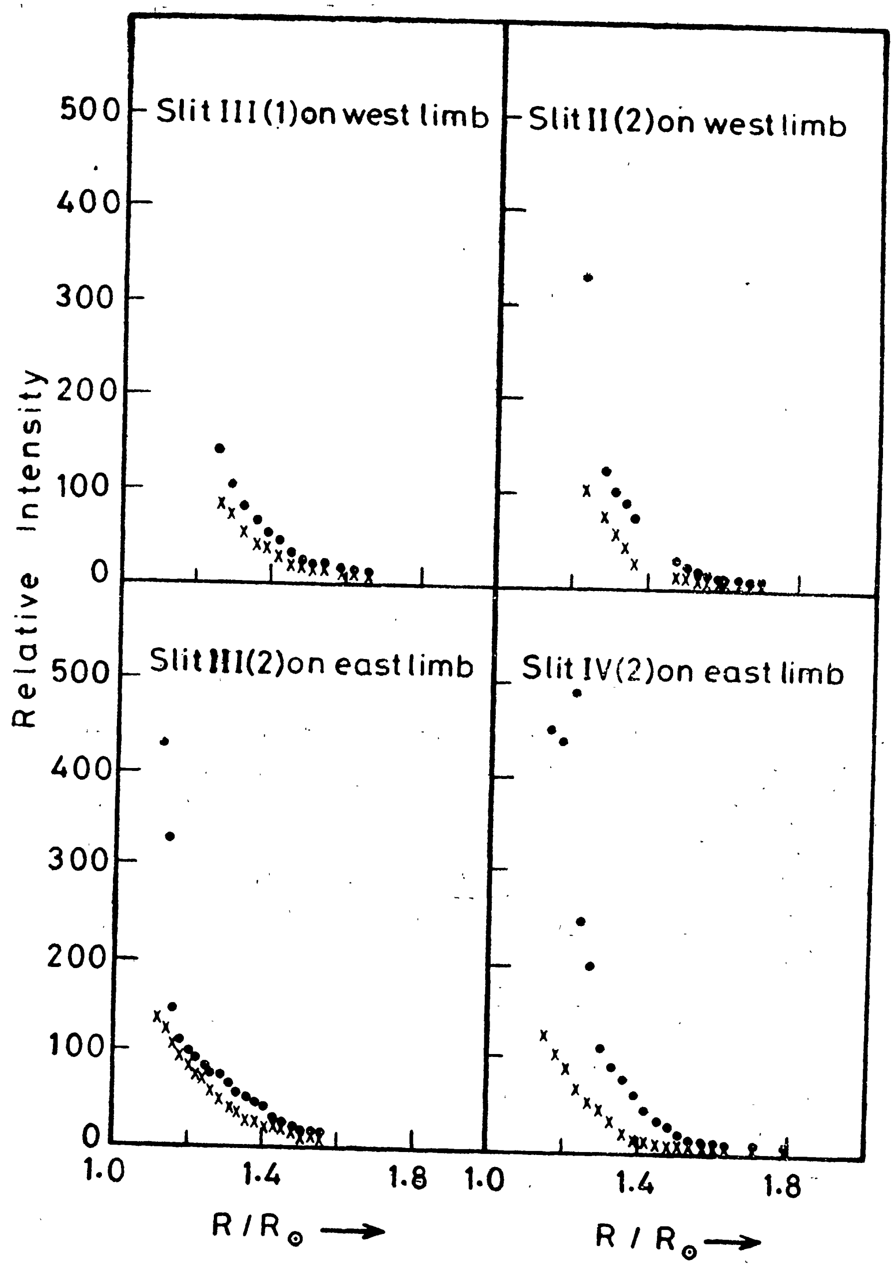

Figure 5. A plot of continuum (crosses) and the [Fe x] line (filled circles) intensity versus radial distance.

The multislit arrangement covers several helmets and streamers and it is possible to choose those locations where the slit has an almost radial orientation. When we do this for the K corona along the locations (a) western part of slits II (2) and III (1) and (b) eastern part of slits III (2) and IV (2) as indicated in Fig. 3, we obtain gradients of intensity shown in Fig. 5 consistent with the trends known to exist in such features over a century of observing eclipses. Coronal emission-line intensities are the straight ratios of Column (8) in Table 1. These conform to the steep gradients of emission lines that we are familiar with. A logarithmic representation is seen in Fig. 6.

© Indian Academy of Sciences • Provided by the NASA Astrophysics Data System

1982JApA....3..249S

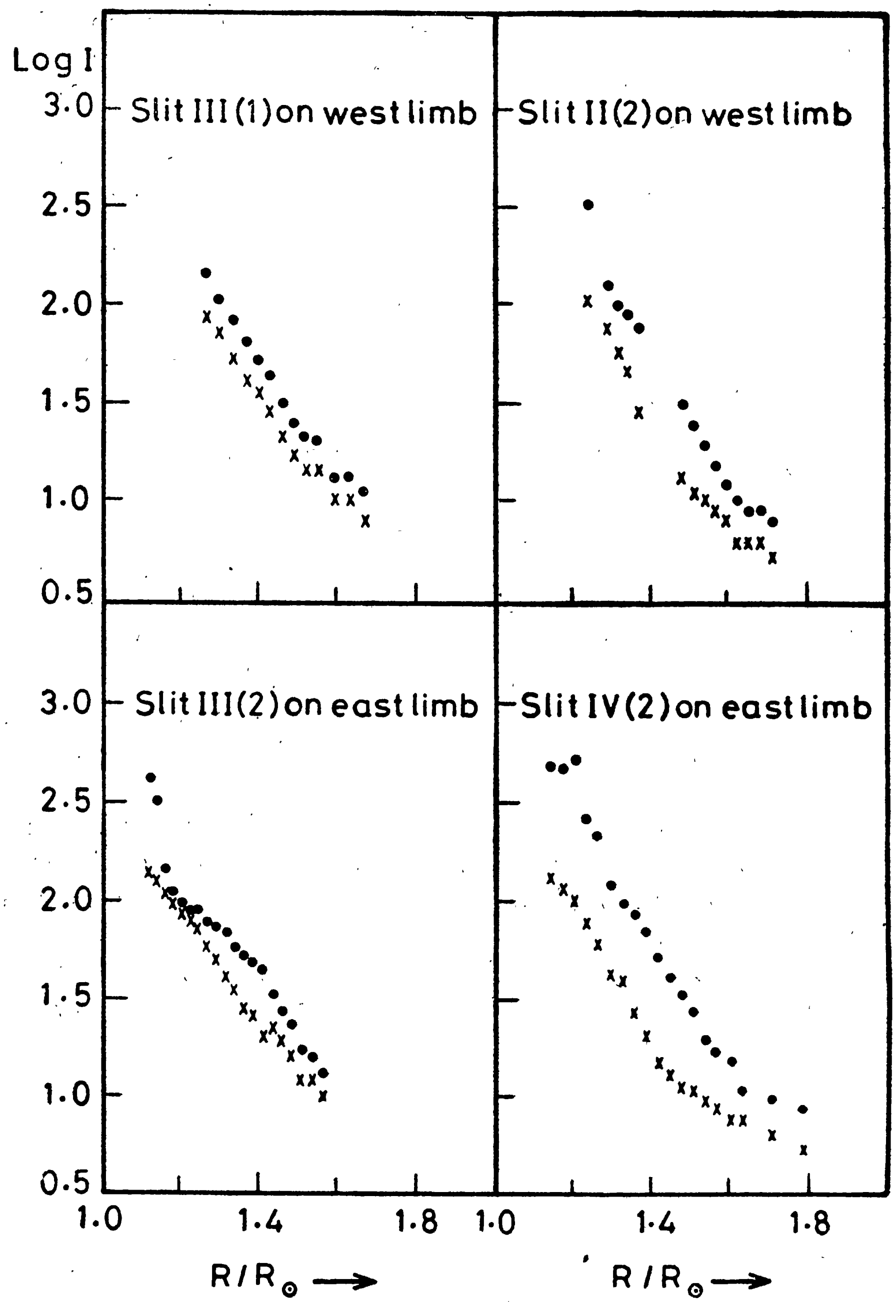

Figure 6. Logarithmic intensity of continuum (crosses) and the [Fe x] line (filled circles) versus radial distance.

4.3 *Coronal Hole and Transient*

A noticeable coronal hole near the south pole was one of the striking features of the 1980 eclipse. We have several measures that cover the position angle range 170°–190°. The tangential slit position restricts the $R/R_\odot$ values from 1·43 to 1·53. A noticeable characteristic of the line widths is that a majority of them have small values. We interpret this to mean that the random motions sampled in this region in the line of sight are of small magnitude, a picture consistent with the open field structure and guided radial plasma outflow over a coronal hole.

© Indian Academy of Sciences • Provided by the NASA Astrophysics Data System

1982JApA....3..249S

Coronal transients are normally rare events to be observed during an eclipse. Such features were observed above the west limb by Japanese observers among others located in Kenya. The region had quietened down by the time moon's shadow had reached India. There is an enhancement near the limb in the white light corona at position angle 106° seen by several teams. K. K. Scaria of Indian Institute of Astrophsics, who obtained high-resolution white-light pictures of the sun in India, reports a filament structure in the position angle range 95° to 118° and at a mean distance of 1·73 $R_\odot$. This filament seems to be remnant of a transient display. The region near the limb continued to be highly disturbed; the highest values of line width of the red line measured anywhere in the corona are found in this region even to large values of $R_\odot$.

4.4 *Line-of-Sight Velocities in the Corona and Coronal Equatorial Rotation*

We have measured radial velocities with the aid of the neon comparison lines, at several points along each slit on both the east and west corona. These values are shown in Table 2 and refer to the solar equator. In particular, slit positions II (1), III (2) and III (1) have been utilized for the rotation measures. The differences amongst the several different values of displacement of the coronal emission line lowers the accuracy of measurement; this is unlike the measures from absorption lines of photospheric origin. We have therefore grouped for each slit position, the east and west values. The mean wavelength of the line is derived from the measures near the north and south poles of the sun. The coronal rotation is thus 2·6 km s^{-1} and is comparable to the photospheric value. The limited accuracy of our measures (probable error $\pm 1{\cdot}5$ km s^{-1}) of faint broad lines only permits a confirmation of co-rotation of the corona.

A distribution of line-of-sight velocities measured all over the corona is displayed in Fig. 7. None of the regions covered by our multislit arrangement show abnormally

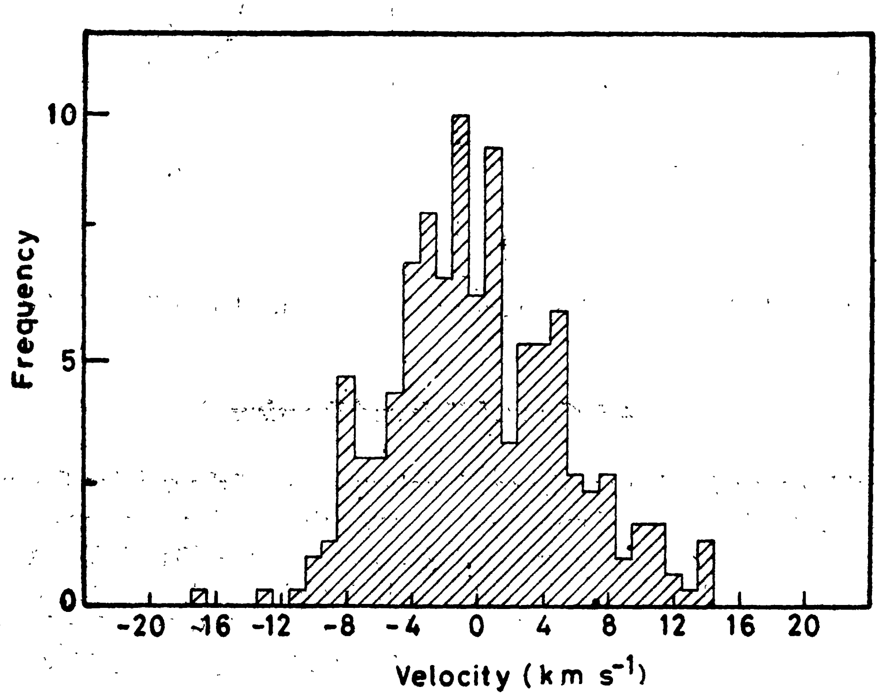

Figure 7. Frequency distribution of line-of-sight velocities as derived from [Fe x] 6374Å line.

© Indian Academy of Sciences • Provided by the NASA Astrophysics Data System

1982JApA....3..249S

large velocities in the corona reported earlier by Delone and Makarova (1969) and for this eclipse by Chandrasekhar, Desai and Angreji (1981). The latter find a splitting of the interference fringe pattern at position angle 256° indicating a component with a line-of-sight velocity of 70 km s^{-1}. This would imply, if confirmed, that there is a mass component with a velocity indicating expansion in perhaps a preferred direction. This region is covered by our slit position II (1), that spans the position angle 252°–257°. Not only do we not see any splitting of the emission line, but we also do not find any abnormal shift even of the line as a whole. The observed velocities are all within the range ± 11 km s^{-1}. However, one should note that we have derived the line-of-sight velocities from the red coronal line sensitive to a region with temperature of $1{\cdot}3 \times 10^6$ K whereas Chandrasekhar, Desai and Angreji (1981) have measured from the green line contributed mostly from regions with a temperature of $2{\cdot}5 \times 10^6$ K.

Table 2. Line-of-sight velocities derived from the red coronal line.

No. (1)	Position angle (2)	$R/R_\odot$ (3)	v km s^{-1} (4)
	Slit IV (1)		
1	320·1	1·495	1
2	321·0	1·475	1
3	321·9	1·456	1
4	322·9	1·437	0
5	323·9	1·418	−5
6	324·9	1·400	−6
7	325·9	1·383	−1
8	327·0	1·365	−2
9	328·1	1·348	0
10	329·2	1·332	1
11	330·3	1·317	−7
12	331·5	1·301	−3
13	332·7	1·287	3
14	333·9	1·273	−1
15	335·2	1·259	0
16	336·5	1·247	−1
17	337·8	1·234	2
18	339·1	1·223	1
19	340·5	1·219	−1
20	341·8	1·202	−1
21	343·2	1·192	0
22	344·7	1·183	1
23	346·1	1·175	−2
24	349·1	1·162	4
25	350·5	1·156	8
26	352·0	1·151	5
27	353·6	1·147	5
28	355·1	1·144	11
29	356·6	1·141	7
30	358·2	1·139	4
31	359·7	1·139	3
32	1·3	1·139	2
33	2·8	1·141	3
34	4·4	1·143	4
35	5·9	1·147	0
36	7·4	1·151	8
37	9·0	1·156	2
38	10·0	1·162	−1
39	12·0	1·168	2
40	13·4	1·175	5
41	14·9	1·183	3
42	16·3	1·192	5
43	17·8	1·202	3
44	19·2	1·212	−1
45	20·5	1·223	1
46	21·9	1·234	1
47	23·2	1·247	−2
48	24·5	1·259	−2
49	25·8	1·273	−2
50	27·1	1·287	−7
51	28·3	1·302	−2
52	29·5	1·317	−3
53	30·7	1·332	−1
54	31·8	1·349	−4
55	32·9	1·365	−8
56	34·0	1·383	1
57	35·1	1·400	−6
58	36·1	1·418	−4
59	37·1	1·437	−1
60	38·1	1·456	−1
61	40·0	1·475	−8
62	40·9	1·495	−5
63	41·8	1·515	−3
64	42·7	1·536	−8
65	43·5	1·557	−3
66	44·3	1·578	−6
67	45·1	1·599	−10
68	45·9	1·621	−3
69	46·6	1·643	−8
70	47·3	1·665	−9

© Indian Academy of Sciences • Provided by the NASA Astrophysics Data System

Table 2. Continued.

No. (1)	Position angle (2)	$R/R_\odot$ (3)	v km s^{-1} (4)
	Slit IV (2)		
71	312·1	1·297	0
72	313·1	1·274	−1
73	314·0	1·251	1
74	315·0	1·229	2
75	316·0	1·207	3
76	317·1	1·186	5
77	318·2	1·165	5
78	319·3	1·145	10
79	320·5	1·125	10
80	53·8	1·440	−7
81	53·0	1·415	−2
82	52·2	1·391	−2
83	51·4	1·367	−1
84	50·6	1·343	0
85	49·8	1·320	−4
86	48·9	1·297	−3
87	48·0	1·274	−1
88	47·0	1·251	−4
89	46·0	1·229	−3
90	45·0	1·208	−3
91	43·9	1·186	−5
92	42·8	1·165	0
93	41·7	1·145	−1
	Slit III (1)		
94	284·2	1·631	1
95	284·4	1·600	−4
96	284·7	1·571	−10
97	285·0	1·541	−2
98	285·3	1·511	0
99	285·6	1·482	−3
100	285·9	1·452	−4
101	286·2	1·422	−4
102	286·5	1·392	1
103	286·9	1·363	0
104	287·3	1·333	−1
105	287·7	1·304	5
106	288·1	1·275	4
107	288·5	1·245	9
108	289·0	1·216	−1
109	289·4	1·187	11
110	289·9	1·158	10
111	290·4	1·129	14
112	77·3	1·690	3
113	77·1	1·660	−4
114	76·9	1·631	−7
115	76·6	1·601	−5
116	76·3	1·571	−9
117	76·0	1·541	−6
118	75·8	1·511	−7
119	75·5	1·482	−4
120	75·1	1·452	−3
121	74·8	1·422	−6
122	74·5	1·393	−4
123	74·1	1·363	−2
124	73·7	1·334	−5
125	73·3	1·304	−4
126	72·9	1·275	−7
127	72·5	1·245	−3
128	72.1	1·216	−6
129	71·6	1·187	0
130	71·1	1·158	1
	Slit III (2)		
131	274·6	1·496	−1
132	274·7	1·465	−3
133	274·8	1·435	−2
134	274·9	1·404	0
135	275·0	1·373	−1
136	275·1	1·343	1
137	275·2	1·312	4
138	275·3	1·281	6
139	275·4	1·251	5
140	275·6	1·220	5
141	275·7	1·189	4
142	86·7	1·619	0
143	86·6	1·588	−2
144	86·5	1·557	−2
145	86·5	1·527	−5
146	86·4	1·496	−3
147	86·3	1·465	−5
148	86·2	1·435	−8
149	86·1	1·404	−8
150	86·0	1·373	−8
151	85·9	1·342	−4
152	85·8	1·312	−3
153	85·7	1·281	−2
154	85·6	1·251	−2
155	85·4	1·220	−4
156	85·3	1·189	−3
157	85·2	1·159	−4
158	85·0	1·128	−4
	Slit II (1)		
159	256·3	1·507	11
160	256·0	1·477	6
161	255·7	1·448	9
162	255·4	1·418	1
163	255·1	1·388	3
164	254·7	1·359	0
165	254·4	1·329	1
166	254·0	1·300	5
167	253·6	1·270	1
168	253·2	1·241	−9
169	252·8	1·211	−3
170	252·3	1·182	−4

© Indian Academy of Sciences • Provided by the NASA Astrophysics Data System

1982JApA....3..249S

1982JApA....3..249S

Table 2. Continued.

No. (1)	Position angle (2)	$R/R_{\odot}$ (3)	v km s^{-1} (4)
171	104·1	1·567	7
172	104·4	1·537	1
173	104·7	1·507	5
174	105·0	1·478	−4
175	105·3	1·448	1
176	105·6	1·418	14
177	106·0	1·388	−7
178	106·3	1·359	−2
179	106·6	1·329	−8
180	107·0	1·300	−3
181	107·4	1·270	−2
182	107·8	1·241	−17
183	108·2	1·211	−11
184	108·7	1·182	−6
185	109·2	1·153	−3
186	109·7	1·124	−10
187	110·2	1·095	−8
	Slit II (2)		
188	247·1	1·626	−3
189	246·6	1·598	−5
190	246·2	1·570	−4
191	245·7	1·542	0
192	245·2	1·514	0
193	244·7	1·486	4
194	244·2	1·459	7
195	242·5	1·376	8
196	241·9	1·349	3
197	241·3	1·322	4
198	240·6	1·296	1
199	239·9	1·269	4
200	239·2	1·242	5
201	238·4	1·216	0
202	237·6	1·190	5
203	117·3	1·431	1
204	117·9	1·404	3
205	118·5	1·376	2
206	119·1	1·349	−1
207	119·7	1·322	1
208	120·4	1·296	0
209	121·1	1·269	1
210	121·8	1·243	−4
211	122·6	1·217	−1
212	123·4	1·190	−8
213	124·2	1·165	−8
214	125·0	1·139	−8
215	126·0	1·114	−4
216	126·9	1·089	1
	Slit I (1)		
217	218·5	1·425	7
218	217·5	1·406	8
219	216·5	1·387	12
220	215·5	1·370	8

No. (1)	Position angle (2)	$R/R_{\odot}$ (3)	v km s^{-1} (4)
221	214·4	1·353	6
222	213·3	1·335	4
223	212·2	1·319	−3
224	211·0	1·303	−6
225	207·4	1·259	−1
226	204·8	1·232	−1
227	202·2	1·208	12
228	198·0	1·177	1
229	195·1	1·160	−2
230	190·6	1·140	1
231	182·9	1·124	4
232	175·0	1·128	−1
233	167·4	1·153	−7
234	165·9	1·160	−13
235	164·5	1·168	−1
236	163·0	1·177	−3
237	161·6	1·187	−8
238	160·2	1·197	−8
239	158·8	1·208	−1
240	157·5	1·220	4
241	156·2	1·232	6
242	154·9	1·245	8
243	153·6	1·259	11
244	152·4	1·273	14
245	151·2	1·288	7
246	150·0	1·303	7
247	148·8	1·319	13
248	147·7	1·335	10
249	146·6	1·353	5
250	145·6	1·370	3
251	144·5	1·387	14
252	143·5	1·406	5
253	142·5	1·425	−1
	Slit I (2)		
254	208·8	1·590	3
255	207·8	1·576	1
256	206·8	1·562	8
257	205·8	1·548	3
258	204·8	1·536	3
259	203·7	1·523	6
260	202·6	1·511	3
261	201·5	1·500	4
262	200·4	1·489	6
263	199·3	1·479	4
264	198·2	1·469	6
265	197·0	1·460	10
266	195·9	1·452	11
267	194·7	1·444	8
268	193·5	1·437	5
269	192·3	1·430	−1
270	191·1	1·424	9
271	189·9	1·419	4
272	188·6	1·414	−7

© Indian Academy of Sciences • Provided by the NASA Astrophysics Data System

1982JApA....3..249S

Table 2. Concluded.

No. (1)	Position angle (2)	$R/R_\odot$ (3)	v km s^{-1} (4)	No. (1)	Position angle (2)	$R/R_\odot$ (3)	v km s^{-1} (4)
273	187·4	1·410	−5	287	167·5	1·437	−4
274	186·1	1·407	−3	288	166·3	1·444	−1
275	184·9	1·404	−3	289	165·1	1·452	2
				290	164·0	1·460	−3
276	183·6	1·402	1				
277	182·4	1·401	0	291	162·8	1·469	−2
278	181·1	1·400	2	292	161·7	1·479	−1
279	179·9	1·400	2	293	160·6	1·489	−2
280	178·6	1·401	5	294	159·5	1·500	−1
				295	158·4	1·511	−6
281	174·9	1·407	7				
282	173·6	1·410	6	296	157·3	1·523	−5
283	172·4	1·414	4	297	156·3	1·535	−9
284	171·1	1·419	3	298	155·2	1·548	−5
285	169·9	1·424	5	299	154·2	1·562	−5
				300	153·2	1·576	−5
286	168·7	1·430	2				

Acknowledgements

We are grateful to T. P. Prabhu for much help both at the eclipse site and later in the reduction of the data. The successful operation of the instrument owes much to the fabrication skill of F. Gabriel, A. Charles and A. Samson.

References

Chandrasekhar, T., Desai, J. N., Angreji, P. D. 1981, *Appl. Opt.*, **20,** 2172.
Delone, A. B., Makarova, E. A. 1969, *Solar Phys.*, **9,** 116.
Jarrett, A. H., von Klüber, H. 1955, *Mon. Not. R. astr. Soc.*, **115,** 343.
Jarrett, A. H., von Klüber, H. 1961, *Mon. Not. R. astr. Soc.*, **122,** 223.
Jordan, C. 1969, *Mon. Not. R. astr. Soc.*, **142,** 501.
Liebenberg, D. H., Bessey, R. J. Watson, B. 1975, *Solar Phys.*, **44,** 345.
Livingston, W., Harvey, J., Doe, L. 1970, *Solar Eclipse 1970 Bulletin F,* National Science Foundation, Washington, p. 72.
Marshall, P. M., Henderson, G. 1973, *Solar Phys.*, **33,** 153.

© Indian Academy of Sciences • Provided by the NASA Astrophysics Data System